Analysis and enhancements of the coolant velocity estimation method in PWR core

Sándor Kiss, Sándor Lipcsei [*]

[a] Centre for Energy Research, P.O. Box 49, Budapest H-1525, Hungary

ABSTRACT

Difficulties of the determination of the coolant velocity in the reactor core are investigated. Global neutron fluctuation and distortion of the detector's transfer function due to its finite size are examined. Cross spectra of the propagating perturbation free from background noise are produced. It is shown that above 1.5 Hz the local component is only visible within 1 to 2 fuel assemblies away from the perturbation and the reactivity term of the fluctuation induced by the perturbation in the detector signal can be neglected. It is also shown that the similarity of the spectra of the background noise and the propagating perturbation results in a sharper peak in the impulse response function. An easy-to-use method is introduced in order to eliminate the effect of the background noise in the determination of the transit time. Additionally, the effect of the axial distribution of the static neutron flux is investigated on the determination of the transit time.

© 2022 The Authors. Published by Elsevier Ltd. This is an open access article under the CC BY license (http://creativecommons.org/licenses/by/4.0/).

1. Introduction

Reactor diagnostics measurements at the Paks VVER-440 reactors have been performed since their start-up. A necessity to directly monitor the coolant velocity distribution by using the neutron detectors of the standard in-core instrumentation was realized during a crud deposition event at Unit 2 in 1997 (Adorján, Czibók, Kiss, Krinizs, & Végh, 2000). Standard in-core instrumentation of pressurized water reactors (PWRs) does not contain detectors for measuring coolant velocity distribution, usually the average core coolant velocity value is determined from the core mass flow rate. In-core thermocouples and neutron detectors allow the velocity to be measured with correlation method (Sweeney, Upadhyaya, & Shieh, 1985). Application of two thermocouples is also known in a research reactor environment (Pór, Berta, & Csuvár, 2003). Other applications and a historical overview can be found in (Pázsit & Demazière, 2010), although most of the applications are in boiling water reactors (BWRs), since the perturbations are much larger in a two-phase flow.

The in-core thermocouples of VVER-440 reactors are too slow (their response time is more than 2.5 s) and they are only placed at the outlet of those fuel assemblies that do not have neutron detector installed. Therefore, the only option to measure the coolant velocity locally in this reactor type is using the installed self-powered neutron detectors (SPNDs) whose signals contain the global background noise in addition to the local effect of the perturbations travelling with the coolant flow. These detectors are Rhodium (Rh) SPNDs having several disadvantages in terms of neutron noise measurement: slowness, low sensitivity above 0.1 Hz, large delayed signal content in addition to the prompt one, distorting effect of the cable current. At the same time the cable current of some detectors with longer cables might compensate the global background noise, helping the velocity estimation (Kiss, Lipcsei, & Házi, 2003).

Neutron fluctuation induced by a perturbation travelling with the coolant through the reactor core can be handled as a global and local component, and the latter allows the coolant velocity to be estimated. These two components were described and their ratio was determined and analysed theoretically in (Kosály, 1975) and (Behringer, Kosály, & Kostić, 1977). The phenomenon was further investigated by using measurements performed in a BWR (Behringer, Kosály, & Pázsit, 1979) and (Kosály, 1980). Neither of the two components supresses the other in BWRs, while the local component may significantly exceed the global one in PWRs (Pázsit & Dykin, 2010).

In normal conditions, transients in the detector signal induced by inhomogeneities travelling with the coolant are so small that the transit time cannot be measured directly. It is due to the global

---

* Corresponding author.
  E-mail address: lipcsei.sandor@ek-cer.hu (S. Lipcsei).

background noise that appears at each point of the reactor core nearly in-phase and practically obscures the local neutron fluctuation induced by the perturbations passing by the detectors. Single perturbations passing through only some fuel assemblies of the core generate such reactivity changes which induce only a small, inseparable but negligible part (attributable to the above mentioned global component) of the (global) background noise.

The present paper analyses the method that has been proven so far for coolant velocity estimation in PWRs (Adorján, Czibók, Kiss, Krinizs, & Végh, 2000) and provides new results regarding the method and the effect of the finite size of the detectors. It is shown that the frequency dependence of the background noise is similar to that of the propagating perturbation component that results in a sharp peak in the impulse response function even in the presence of the background noise. Additionally, an enhancement of the method is introduced that simplifies the identification of the transit time peaks. The results are demonstrated with measurements carried out in a VVER-440 reactor unit.

Our investigation of the model of the coolant velocity estimation mainly focuses on how the properties of the temperature perturbations (δT) travelling with the coolant show in the detector signals (see the scheme of the coolant flow in a VVER-440 reactor vessel in Fig. 1, left). For simplicity, external mechanical and electronic influences (like in-core mechanical vibrations, pressure waves, mains frequency, electronic influence of mechanical equipment, etc.) appearing in the detector signals are not investigated.

The core of a VVER-440 reactor consists of 349 shrouded, hexagonal fuel assemblies; 36 assemblies contain detector chains placed in their central instrumentation tube. The radial arrangement of the detector in the active core is shown in the central part of Fig. 1. This figure also shows the locations of the detector chains selected for the measurements that will be discussed later in Section 3. Each detector chain consists of 7 uncompensated Rh SPNDs and a so called compensation cable which can be used as background detector (see Fig. 1, right).

The coolant velocity measurement is facilitated by the presence of the fuel assembly shrouds as they prevent cross assembly coolant flow, thus a perturbation entering in a fuel assembly goes

through it and its effect is sensed by the detectors of the chain associated with the assembly.

The VVER-440 reactor has six primary circulating loops with approximately 50% coolant mixing (Elter, 2005). The fluctuation of the primary coolant is significantly dampened in the steam generators, fluctuations of the hot leg are practically suppressed above 1.5 Hz (Kiss & Lipcsei, 2014), (Kiss & Lipcsei, 2015). Consequently, coolant perturbations entering the fuel assemblies are small and nearly independent above 1.5 Hz and the contribution of these perturbations to the whole background noise can be neglected.

The paper contains several spectra of SPND signals measured in Unit 2 of Paks plant. These measurements were performed by means of the PAZAR noise data acquisition system (Lipcsei, Kiss, & Czibók, 2004) with 100 Hz sampling rate. The spectral functions were estimated by using 1024-point Fast Fourier Transforms of 1 h long measurements, resulting in more than 700 sweeps with 50% overlap. Hanning windows were applied for data smoothing.

In this paper we perform our investigation in terms of measurement. The various phenomena (propagating perturbation and induced noise, global background noise) are all grouped in terms of measurement and described by separate transfer function. In Section 2 we investigate how a propagating perturbation travelling along a finite length detector can be measured in the presence of in-phase background noise. In the longest Section 3 we introduce a third detector to the model in order to separate the perturbation and background noise in the measured signals, and then the spectra of the separated components are investigated. In Section 4 we show the usual way of determining the transit time based on cross-correlation, and additionally we introduce a novel method that results in a more easily identifiable peak in the cross correlation functions. In order to specify the transfer function of the detector for propagating perturbation, an already known simple neutron physics model is used in Section 5. In Section 6 we show how this transfer function is influenced by the different size of the cable and the detector, and the transfer function of an uncompensated detector is derived, as well. In Section 7 we investigate the effect of the axially non-constant neutron flux on the transfer function of the neutron detector for propagating perturbation,
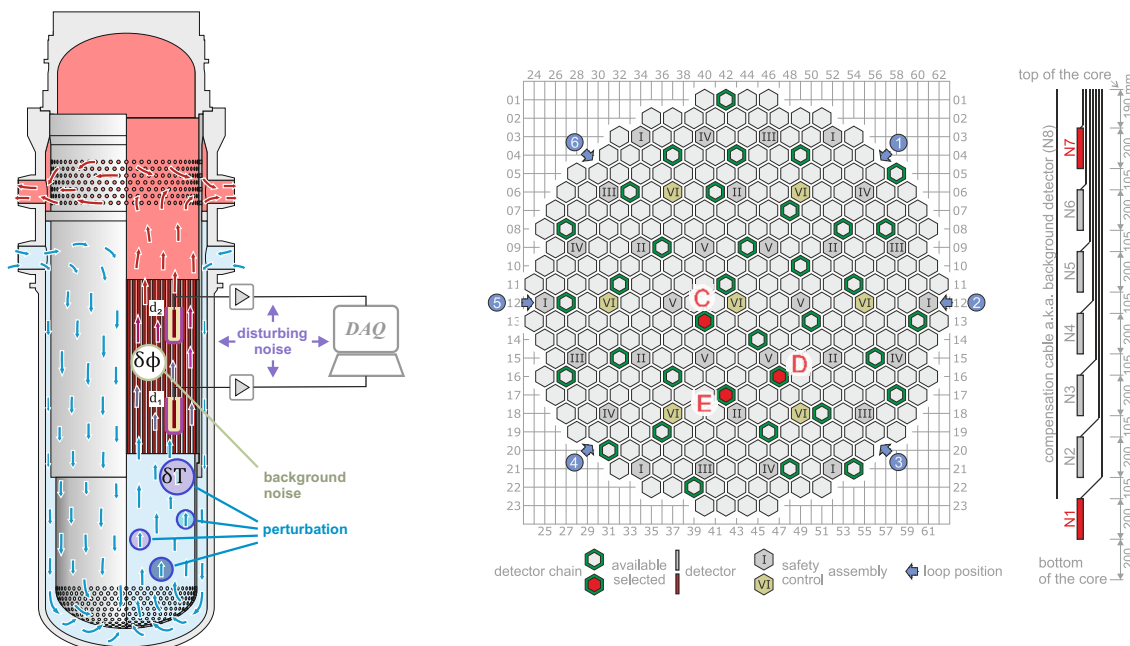

Fig. 1. Scheme of the coolant flow in the reactor (left) and radial and axial arrangement of the neutron detectors in the core (centre and right, respectively).

while Section 8 illustrates how the same condition influences the measurement of transit time.

2. Transfer function of the measurement of a propagating perturbation

The velocity of the coolant is estimated by measuring the transit time of the perturbations travelling with the coolant between two detectors placed in the flow (note that the distance between the detectors is known). The measured signals have to be corrected for the transfer properties of the measurement system, i.e. for the distortions caused by the detector and the measuring instrumentation. The simplest model of the measurement is shown in Fig. 2, where the instrumentations are assumed to be identical (it is true for the presented measurements due to the characteristics of the instrumentation used, but it has to be considered when they are not identical).

A $\delta\varphi_1(\omega)$ perturbation at position z_1 appears at position z_2 with τ_{12} time delay, which is described by the transfer function $H_{12}(\omega)$:

$$\delta\varphi_2(\omega) = H_{12}(\omega)\delta\varphi_1(\omega) = e^{-i\omega\tau_{12}}\delta\varphi_1(\omega) \quad (1)$$

The signals measured in the detectors are:

$$\delta I_1(\omega) = H_1(\omega)H_a(\omega)\delta\varphi_1(\omega)$$

$$\delta I_2(\omega) = H_2(\omega)H_a(\omega)\delta\varphi_2(\omega) \quad (2)$$

The transfer function of the propagation of the perturbation can be expressed using (1) as:

$$H_{12}(\omega) = \frac{\delta\varphi_2(\omega)}{\delta\varphi_1(\omega)} = \frac{H_1(\omega)\delta I_2(\omega)}{H_2(\omega)\delta I_1(\omega)}$$

The transfer function between the measured signals can be estimated by using the auto and cross power spectral density functions (APSD and CPSD, respectively):

$$TR_{12}(\omega) = \frac{CPSD_{12}(\omega)}{APSD_1(\omega)} \quad (3)$$

where.

$$CPSD_{12}(\omega) = \left\langle \delta I_1(\omega), \overline{\delta I_2(\omega)} \right\rangle, \quad (4)$$

$$APSD_1(\omega) = \left\langle \delta I_1(\omega), \overline{\delta I_1(\omega)} \right\rangle \quad (5)$$

and overbar denotes complex conjugate. After substitutions (note that the transfer functions of the identical measurement equipment are eliminated).

$$TR_{12}(\omega) = \frac{\overline{H_2(\omega)}}{\overline{H_1(\omega)}}\overline{H_{12}(\omega)},$$

from which the measurement estimation of the $H_{12}(\omega)$ transfer function can be expressed:

$$H_{12}(\omega) = \frac{H_1(\omega)}{H_2(\omega)}\frac{\overline{CPSD_{12}(\omega)}}{APSD_1(\omega)} \quad (6)$$

Since the neutron detectors of the reactor core also detect an in-phase background noise, the model of the measurement is extended accordingly (see Fig. 3).

The transfer function $H_{BG}(\omega)$ of a Rhodium SPND regarding the background noise is nearly constant at $\omega > 0.01$ Hz (Kiss & Lipcsei, 2017). Signals measured by the detectors based on the model of Fig. 3 are:

$$\delta I_1(\omega) = H_1(\omega)H_a(\omega)\delta\varphi_1(\omega) + H_{BG}(\omega)H_a(\omega)\delta\varphi_{BG}(\omega)$$

$$\delta I_2(\omega) = H_2(\omega)H_a(\omega)\delta\varphi_2(\omega) + H_{BG}(\omega)H_a(\omega)\delta\varphi_{BG}(\omega)$$

After substituting them in (3) the transfer function between the measured signals can be written as:

$$TR_{12}(\omega) = \frac{H_1(\omega)\overline{H_2(\omega)}\left\langle\delta\varphi_1(\omega),\overline{\delta\varphi_2(\omega)}\right\rangle + |H_{BG}(\omega)|^2 APSD_{BG}(\omega)}{|H_1(\omega)|^2\left\langle\delta\varphi_1(\omega),\overline{\delta\varphi_1(\omega)}\right\rangle + |H_{BG}(\omega)|^2 APSD_{BG}(\omega)} \quad (7)$$

where it was used that $\delta\varphi_1$ and $\delta\varphi_2$ were independent from $\delta\varphi_{BG}$. When detectors of the same type and size are placed in a neutron flux which is constant along the detectors, then:

$$\frac{H_1(\omega)}{H_2(\omega)} = 1.$$

Substituting this and (1) into (7):

$$TR_{12}(\omega) = \overline{H_{12}(\omega)}\frac{|H_1(\omega)|^2 APSD_\varphi(\omega)}{|H_1(\omega)|^2 APSD_\varphi(\omega) + |H_{BG}(\omega)|^2 APSD_{BG}(\omega)}$$

$$+ \frac{|H_{BG}(\omega)|^2 APSD_{BG}(\omega)}{|H_1(\omega)|^2 APSD_\varphi(\omega) + |H_{BG}(\omega)|^2 APSD_{BG}(\omega)} \quad (8)$$

where $APSD_\varphi(\omega) = \left\langle\delta\varphi_1(\omega),\overline{\delta\varphi_1(\omega)}\right\rangle = \left\langle\delta\varphi_2(\omega),\overline{\delta\varphi_2(\omega)}\right\rangle$ based on (1). The transfer function (8) can be written in the form of:

$$TR_{12}(\omega) = \overline{H_{12}(\omega)}A(\omega) + B(\omega), \quad (9)$$

where $A(\omega)$ and $B(\omega)$ are determined by the propagating perturbation and the background noise, respectively:

$$A(\omega) = \frac{|H_1(\omega)|^2 APSD_\varphi(\omega)}{|H_1(\omega)|^2 APSD_\varphi(\omega) + |H_{BG}(\omega)|^2 APSD_{BG}(\omega)} \quad \text{and}$$
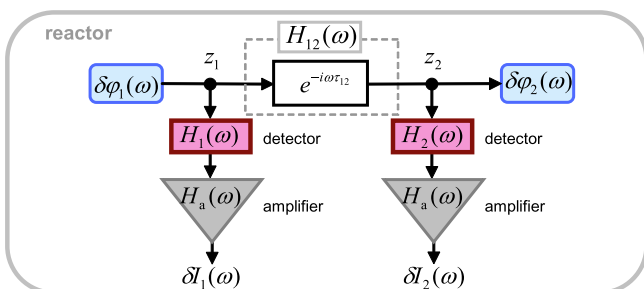

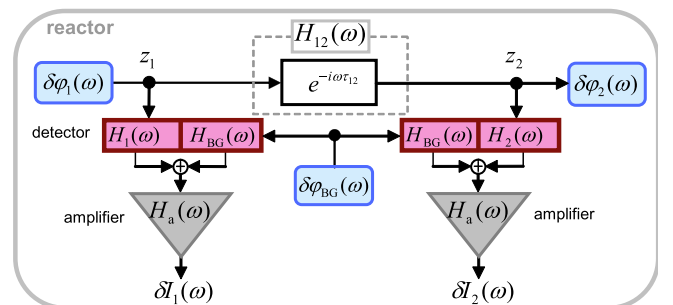**Fig. 2.** Measurement of a perturbation passing by two detectors.

Fig. 3. Measurement of a perturbation passing by two detectors with common background noise.

$$B(\omega) = \frac{|H_{BG}(\omega)|^2 APSD_{BG}(\omega)}{|H_1(\omega)|^2 APSD_\varphi(\omega) + |H_{BG}(\omega)|^2 APSD_{BG}(\omega)} \quad (10)$$

The form of (8) shows that the transfer function $H_{12}(\omega)$ can easily be expressed from the measured transfer function only when the background noise is negligible, i.e. when $B(\omega) = 0$, and consequently $A(\omega) = 1$. Therefore, in the following chapter the ratio of the background noise and the propagating perturbation is examined.

3. The ratio of the propagating perturbation and the background noise

In order to estimate the ratio of the $APSD_\varphi(\omega)$ perturbation and the $APSD_{BG}(\omega)$ background noise by separating the signal contents, the signal of an appropriate third detector is used. In the signal of this third detector the effect of the perturbation passing by the investigated detectors must be negligible, therefore the detectors belonging to a chain which is located in a radial distance of 3–5 fuel assemblies from the investigated chain will suffice for this purpose.

For these investigations the signals of the bottom (N1) and top (N7) detectors are selected because the signal of detector N1 can be compensated by subtracting the signal of the background detector (the compensated signal will be denoted as N1c), In addition, N7 has the shortest cable thus it is subjected to the smallest disturbing effect of the cable. This cable passes through only the topmost part of the core and the upper reflector, its length is only 10–15% of the longest cable belonging to N1. However, its effect cannot be fully eliminated.

For an easier comparison, such detector chains were chosen (see Fig. 1, centre, red markers) which are placed in nearly the same neutron flux (with deviation less than 10%). Additional uncertainty comes from the approximately known prompt ratio of the detectors: it is $(6 \pm 1)\%$ of the DC signal (Tsimbalov, 1984), which represents a relative error of about 16.7%. In order to achieve better statistics we investigated all possible combinations based on the N1 and N7 detectors of the selected three chains (marked with 'C', 'D' and 'E' in the centre Fig. 1). The axial distance between N1 and N7 is 1830 mm (see Fig. 1), and the radial pitch of the fuel assemblies is 147 mm (so the distances between the selected radial locations are: C-D: 641 mm, D-E: 389 mm, E-C: 530 mm).

3.1. Modell for separating the signal contents

Fig. 4 shows the detectors of two arbitrary chains (the odd indices denote the N1 bottom detectors, while the even indices
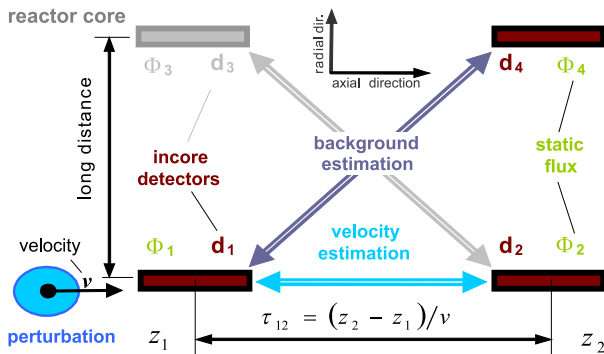

Fig. 4. Estimating the ratio of the background noise and the propagating perturbation.

denote the N7 top ones). When the transit time is calculated from the signals of d_1 and d_2, either d_3 or d_4 can be used as a third detector. Additionally, the role of the chains is interchangeable.

In order to investigate the cross spectra between the detectors, coherences and phases are shown in Fig. 5 between the diagonal detectors ("background estimation" in Fig. 4) in all possible pairs of the three selected detector chains.

Coherences and phases between detectors of the same fuel assemblies are shown in Fig. 6. Behaviour of the measured neutron noise signals is not investigated in the frequency range under 1.5 Hz, because it is determined by feedbacks and reactor control. The phase is definitely around zero with 40% coherence above 1.5 Hz in the diagonal spectra (Fig. 5), consequently no sign of propagating perturbation can be seen. The phase behaviour above 1.5 Hz between the detector signals of the same chain (same fuel assembly) with high coherence having a sink structure clearly suggests the presence of propagating perturbation. The sink structure will be explained later based on (17). Such a sink structure is also presented in Fig. 16 of (Pázsit & Demazière, 2010).

Flowchart of the model of Fig. 4 is presented in Fig. 7.

The following applies to the model:

a) The measurement circuits connected to the detectors are considered ideal, their transfer function is $H_a(\omega) = 1$.

b) $\Phi_1 = \Phi_2 = \Phi_3 = \Phi_4$ (this assumption is satisfied within 10% for the selected signals), where $\Phi_i = \varphi_0(z_i), i = 1, \cdots, 4$, is the value of the static neutron flux at the i-th detector position.

c) Transfer functions of the identical detectors are equal to each other: $H_1(\omega) = H_2(\omega) = H_3(\omega) = H_4(\omega)$.

d) Regarding the prompt signal content: $H_{BG}(0) = H_1(0)$ and $H_{BG}(\omega) = \text{const}$.

e) Due to the symmetrical arrangement $H_{12}(\omega) \approx H_{34}(\omega)$, $H_{13}(\omega) \approx H_{31}(\omega)$ and $H_{14}(\omega) = H_{32}(\omega)$.

f) Since there is no cross flow, the effect of the perturbation entering the bottom of an assembly on the top detector of any other chain is determined by the same delay: $H_{14}(\omega) \approx c \cdot H_{12}(\omega)$, where $c \leq 1$.

g) In our measurements there is no sign of propagating perturbation of common source between detectors placed at a radial distance of three fuel assemblies (see Fig. 5 and Fig. 1), that is even the radially closest detectors do not sense the perturbations travelling between them. It is important to emphasize that in practice this means that the perceptibility (or detector field of view) of the local component of the perturbations above 1.5 Hz is limited to 1–2 fuel assemblies. Hence $\delta\varphi_1(\omega)$ and $\delta\varphi_3(\omega)$ are independent for the selected chains, that is $\langle\delta\varphi_1(\omega), \delta\varphi_3(\omega)\rangle = 0$. The power spectra of the inlet perturbations are nearly identical for symmetry reasons, i.e. $APSD_{\varphi_1}(\omega) \approx APSD_{\varphi_3}(\omega)$.

h) The contribution from the reactivity term to the noise induced by the fluctuation is negligible in large systems and/or at high frequencies for propagating perturbations (Pázsit & Dykin, 2010), therefore $|CPSD_{\varphi BG}(\omega)| \ll APSD_\varphi(\omega)$.

3.2. Separation of the spectra of the background and the perturbation

Now the $\delta I_i(\omega)$ currents can be written based on the flowchart of Fig. 7. First the currents of the two detectors used to measure the propagating perturbation:

$$\delta I_1(\omega) = H_1(\omega)\delta\varphi_1(\omega) + H_{BG}(\omega)\delta\varphi_{BG}(\omega) + H_{31}(\omega)\delta\varphi_3(\omega),$$

$$\delta I_2(\omega) = H_{12}(\omega)H_2(\omega)\delta\varphi_1(\omega) + H_{BG}(\omega)\delta\varphi_{BG}(\omega) + H_{31}(\omega)\delta\varphi_3(\omega)$$
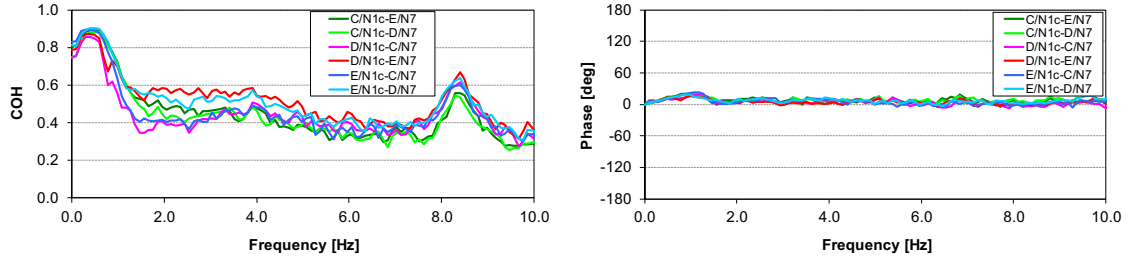
and the third detector used to determine the background:

Fig. 5. Coherences and phases between diagonal detectors (between the N1 bottom and N7 top detectors of different chains; N1c signals are compensated).
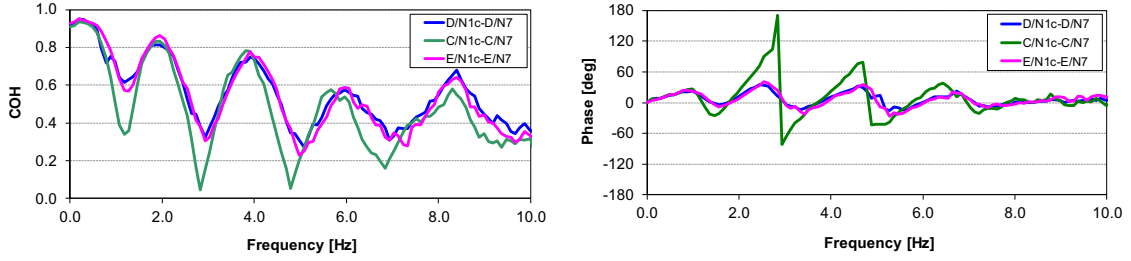

Fig. 6. Coherences and phases between detectors of the same fuel assemblies (between the N1 bottom and N7 top detectors of the same chains, N1c signals are compensated).
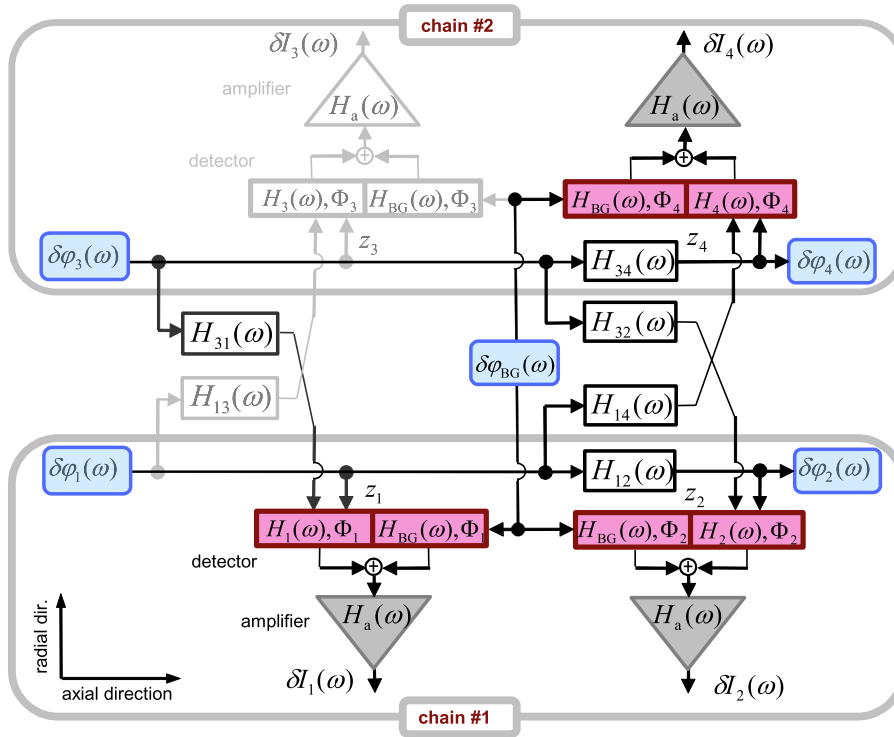

Fig. 7. Connections between the detectors of two chains.

$$\delta I_4(\omega) = H_{34}(\omega)H_4(\omega)\delta\varphi_3(\omega) + H_{BG}(\omega)\delta\varphi_{BG}(\omega) + H_{14}(\omega)\delta\varphi_1(\omega)$$

Selecting $\delta I_4(\omega)$ is arbitrary, $\delta I_3(\omega)$ would be just as good.

$$NAPSD_1(\omega) = \langle \delta I_1(\omega), \delta I_1(\omega)\rangle$$

Since $\delta\varphi_1(\omega)$ and $\delta\varphi_3(\omega)$ are independent (see *item g* in the above list) and $\langle \delta\varphi_i(\omega), \delta\varphi_{BG}(\omega)\rangle$ are negligible (see *item h*), only three terms remain after the multiplication:

$$NAPSD_1(\omega) = \frac{|H_1(\omega)|^2 APSD_{\varphi_1}(\omega)}{\Phi_1^2} + \frac{|H_{BG}(\omega)|^2 APSD_{BG}(\omega)}{\Phi_1^2}$$
$$+ |H_{31}(\omega)|^2 \frac{|H_1(\omega)|^2 APSD_{\varphi_1}(\omega)}{\Phi_1^2}$$

Similarly.

$$NCPSD_{12}(\omega) = \langle \delta I_1(\omega), \delta I_2(\omega)\rangle$$

that is.

$$NCPSD_{12}(\omega) = \overline{H_{12}(\omega)}\frac{|H_1(\omega)|^2 APSD_{\varphi_1}(\omega)}{\Phi_1\Phi_2} + \frac{|H_{BG}(\omega)|^2 APSD_{BG}(\omega)}{\Phi_1\Phi_2}$$
$$+ H_{31}(\omega)\overline{H_{32}(\omega)}\frac{|H_1(\omega)|^2 APSD_{\varphi_1}(\omega)}{\Phi_1\Phi_2}$$

Phase and coherence between the signals can be formed in the usual way:

$$PH_{12}(\omega) = \arg(NCPSD_{12}(\omega)) \tag{11}$$

$$COH_{12}(\omega) = \frac{|NCPSD_{12}(\omega)|}{\sqrt{NAPSD_1(\omega) \cdot NAPSD_2(\omega)}} \tag{12}$$

Due to the symmetrical arrangement (*item e*) and since the phase indicating propagating perturbation does not appear between the detectors of different chains, it suggests that:

$$|H_{12}(\omega)| \gg |H_{13}(\omega)| \approx |H_{31}(\omega)| \approx |H_{14}(\omega)| \approx |H_{32}(\omega)|$$

It follows that the cross spectrum between the opposing detectors contains approximately only the background spectrum, i.e.

$$NCPSD_{14}(\omega) \approx \frac{|H_{BG}(\omega)|^2 APSD_{BG}(\omega)}{\Phi_1\Phi_4} \tag{13}$$

and

$$NAPSD_i(\omega) \approx \frac{|H_i(\omega)|^2 APSD_{\varphi_i}(\omega)}{\Phi_i^2} + \frac{|H_{BG}(\omega)|^2 APSD_{BG}(\omega)}{\Phi_i^2}, i = 1, 2. \tag{14}$$

Phase behaviour of propagating perturbations in an environment nearly free from background noise produced in this way is shown in the right side of Fig. 8.

The corrected coherence (see Fig. 8 left) between the same signals was produced similarly to the above procedure by the following formula:

$$COH_{12}^{(corr)}(\omega)$$
$$= \frac{\left|NCPSD_{12}(\omega) - \frac{\Phi_4}{\Phi_2}NCPSD_{14}(\omega)\right|^2}{\left(NAPSD_1(\omega) - \frac{\Phi_4}{\Phi_1}NCPSD_{14}(\omega)\right)\left(NAPSD_2(\omega) - \frac{\Phi_4}{\Phi_2}NCPSD_{14}(\omega)\right)}$$

The cross spectra between opposing detectors (in the denominator of the above formula) is nearly real (as Fig. 5 shows), however, in practical calculations its real part or absolute value is worth using.

It is important to emphasize that the relative error of the background subtraction can be especially big for small perturbations compared to the background, hence the compensation is mainly an estimation for demonstration. Note that the factor of the background to be subtracted was optimized for the best linear phase in Fig. 8, however, this alteration was always less than 10% and did not change the character of the spectra, but it emphasized the point better: recovery of the phase behaviour of the propagating perturbation is clearly visible when comparing the graphs in Fig. 8 to Fig. 6.

Dependence of the coherence from the ratio of the background and the perturbation can be expressed substituting (14) and (15) in (12):

$$COH_{12} \approx \sqrt{\frac{|H_1|^4 APSD_{\varphi_1}^2 + |H_{BG}|^4 APSD_{BG}^2 + 2|H_1|^2|H_{BG}|^2 APSD_{\varphi_1} APSD_{BG}\cos(\omega\tau_{12})}{|H_1|^4 APSD_{\varphi_1}^2 + |H_{BG}|^4 APSD_{BG}^2 + 2|H_1|^2|H_{BG}|^2 APSD_{\varphi_1} APSD_{BG}}} \tag{17}$$

$$NCPSD_{12}(\omega) \approx \overline{H_{12}(\omega)}\frac{|H_1(\omega)|^2 APSD_{\varphi_1}(\omega)}{\Phi_1\Phi_2}$$
$$+ \frac{|H_{BG}(\omega)|^2 APSD_{BG}(\omega)}{\Phi_1\Phi_2} \tag{15}$$

By multiplying (13) with an appropriate constant and subtracting it from (14) and (15), the term containing the background can be eliminated. E.g.:

$$NCPSD_{12}(\omega) - \frac{\Phi_4}{\Phi_2}NCPSD_{14}(\omega) = \overline{H_{12}(\omega)}\frac{|H_1(\omega)|^2 APSD_{\varphi_1}(\omega)}{\Phi_1\Phi_2} \tag{16}$$

where frequency dependence of spectra and transfer functions was not denoted for clarity and we used that $H_{12}(\omega) = e^{-\omega\tau_{12}}$, $H_2(\omega) = H_1(\omega)$ and $APSD_{\varphi_2}(\omega) = APSD_{\varphi_1}(\omega)$. The above expression shows that coherence is equal to 1 when there is no background noise (or a constant value less than 1 due to other independent noises which may be present in reality), while a waving appears in the coherence with finite background noise and it takes the lowest values at the minimum of the cosine function, i.e. at.

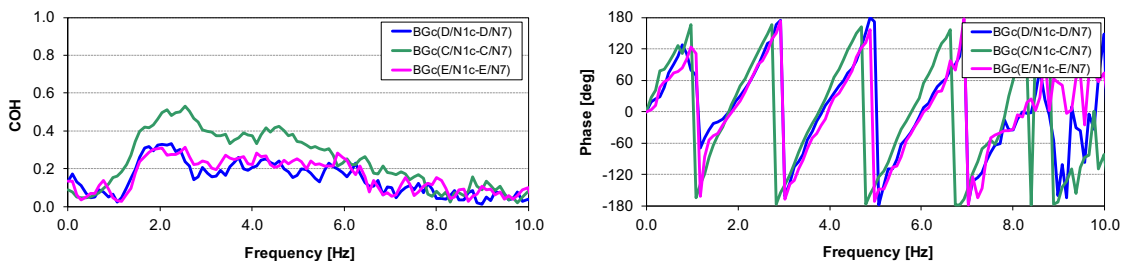$$\omega = \frac{(2n-1)\pi}{\tau_{12}}, n = 1, 2, \cdots,$$

Fig. 8. Coherences and phases modified with background subtraction between detector signals of the same fuel assembly (BGc in legend denotes that the spectrum is background corrected).

Table 1
Zero points of the coherence between detectors N1 and N7 in different chains.

assembly label	coordinate of assembly	velocity [m/s]	frequencies of coherence minimums [Hz]				
			1	2	3	4	5
C	13–40	3.48	0.95	2.85	4.75	6.66	8.56
D	16–47	3.60	0.98	2.95	4.92	6.89	8.85
E	17–42	3.67	1.00	3.01	5.01	7.02	9.02

where.

$$\tau_{12} = \frac{l_{N1-N7}}{v}$$

and v denotes the coolant velocity (in m/s) in the fuel assembly and $l_{N1-N7} = 1.83$ m stands for the distance between detectors N1 and N7 (see Fig. 1, right side).

The first five zero points of the coherences between N1 and N7 in the selected detector chains are listed in Table 1. Minimum locations of coherences in Fig. 6 are in good agreement with the values listed in the Table.

Auto spectra of the background noise and of the perturbation can be expressed from (13) and (16), respectively:

$$APSD_{BG}(\omega) \approx \frac{\Phi_1 \Phi_4 NCPSD_{14}(\omega)}{|H_{BG}(\omega)|^2}$$

$$APSD_{\varphi_1}(\omega) \approx \frac{1}{|H_1(\omega)|^2} |\Phi_1 \Phi_2 NCPSD_{12}(\omega) - \Phi_1 \Phi_4 NCPSD_{14}(\omega)|$$

The spectra calculated (separated) in this way are presented in Fig. 9, where $|H_1(\omega)| = \left|\frac{2v}{\omega L} \sin \frac{\omega L}{2v}\right|$ is assumed and v stands for the velocity of the propagating perturbation and L denotes the length of the detector. This shape of the transfer function will be derived and explained later in Section 5, at Eq. (34).

Both power spectra are characterized by a similar decrease (a shape of $\frac{1}{k^2 + \omega^2}$, where k is constant) in the range between 1.5 and 7.0 Hz. The wide peak at around 8.5 Hz in the spectrum of the background comes from the eigenfrequency of the pressure fluctuation of the primary loop.

Note that when $|H_1|^2 APSD_{\varphi_1}$ and $|H_{BG}|^2 APSD_{BG}$ are equal (this condition is approximately satisfied for the detectors of chain 'C' (or chain 13–40 with its coordinates) between 2 and 6 Hz in Fig. 9, green graph) then COH_{12} of (17) is exactly zero at the minimums of $\cos(\omega\tau_{12})$ (see Fig. 6, left, green graph). In general, the smaller the background to perturbation ratio (or more exactly the background to the effect of the perturbation ratio), the clearer the linear phase at the right graphs of Fig. 6.

3.3. Investigation of the components of the transfer function

We can now investigate the two terms of the transfer function (8). Using (13), (14) and (15) they can be expressed with measured functions:
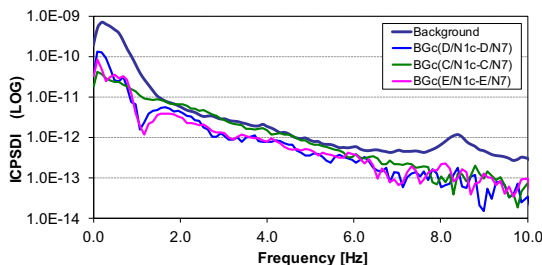

Fig. 9. Separated auto spectra of the background and the perturbation (BGc in legend denotes that the spectrum is background corrected).

$$B(\omega) = \frac{\Phi_4}{\Phi_1} \frac{NCPSD_{14}(\omega)}{NAPSD_1(\omega)} = TR_{14}(\omega) \quad (18)$$

$$\overline{H_{12}(\omega)}A(\omega) = \frac{NCPSD_{12}(\omega)\Phi_1\Phi_2}{NAPSD_1(\omega)\Phi_1^2} = TR_{12}(\omega) - TR_{14}(\omega) \quad (19)$$

Now the terms $\overline{H_{12}(\omega)}A(\omega)$ and $B(\omega)$ can directly be expressed from the measurement, thus the two parts determined by the perturbation and the background of transfer function $TR_{12}(\omega)$ can be separated and investigated. Their absolute values are shown in Fig. 10. In these graphs a slow slope, nearly linear decrease can be observed.

It can be seen – based on the left graph of Fig. 10 – that above 1.5 Hz the contribution of the perturbation to the background noise is negligible in our measurements. The left graph (showing the transfer functions between the signals of opposite detectors) contains plots that all have values under 0.5. The figure shows all possible opposite combinations based on the selected detector chains. Note that all these transfer functions are pure real according to the nearly zero phase of them presented in the left side of Fig. 5. From (18) and the second expression of (10):

$$TR_{14}(f > 1.5 \text{ Hz}) = \frac{|H_{BG}(\omega)|^2 APSD_{BG}(\omega)}{|H_1(\omega)|^2 APSD_\varphi(\omega) + |H_{BG}(\omega)|^2 APSD_{BG}(\omega)} < a$$
$$= 0.5$$

After rearrangement.

$$APSD_{BG}(\omega) < \frac{a}{1-a} \frac{|H_1(\omega)|^2}{|H_{BG}(\omega)|^2} APSD_\varphi(\omega).$$

The first fraction is 1 (or smaller when $a < 0.5$), while the second fraction is nearly 1 or smaller, thus the spectrum of the background noise is smaller than the spectrum of the perturbation above 1.5 Hz.

The background noise consists of several components (see *item g*):

$$APSD_{BG}(\omega) = APSD_{BG}^{\rho_1}(\omega) + \sum_{i=2}^{N} APSD_{BG}^{\rho_i}(\omega) + APSD_{BG}^{+}(\omega),$$

where $N \gg 1$ is the number of independent perturbations going through the different fuel assemblies of the reactor core, $APSD_{BG}^{\rho_i}(\omega) \approx APSD_{BG}^{\rho_1}(\omega)$ denote the spectra of the reactivity fluctuations induced by the perturbations and $APSD_{BG}^{+}(\omega)$ stands for the spectrum of the reactivity change independent from the propagating perturbations. Consequently, the contribution of a single perturbation to the reactivity fluctuation is negligible compared to the whole, and consequently it is much smaller than the spectrum of the perturbation.

$$APSD_{BG}^{\rho_1}(\omega) \ll APSD_\varphi(\omega).$$

$|CPSD_{\varphi BG}(\omega)| \ll APSD_{BG}(\omega)$ when $\omega > 1.5$ Hz. The global background noise is partly made up by the contributions from the various perturbations going through hundreds of fuel assemblies. Hence the contribution from a single channel is negligible compared to the total.
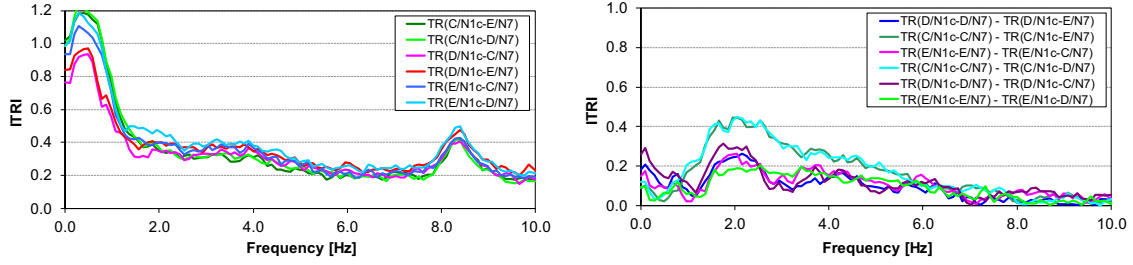
Fig. 10. Absolute value of the two components of the $TR_{12}(\omega)$ transfer function (left: $B(\omega)$, right $\overline{H_{12}(\omega)}A(\omega)$) (the legend shows how these amounts are calculated based on (18) and (19), respectively).

This confirms the approximation of *item h* for the VVER-440 reactor: the contribution from the reactivity term of the fluctuation (compared to the whole) in the detector signal is negligible above 1.5 Hz at 2.5 m reactor height. This value is slightly lower than the value of 2.8 Hz resulting from the theoretical model by (Pázsit & Dykin, 2010). Their Figs. 2 and 16 show that the contribution can be neglected approximately from the first sink, which occurs at 2.8 Hz for a VVER-440 reactor based on their Eq. (33).

4. Determining the transit time of a propagating perturbation

A well identifiable peak appears in the cross correlation function $CCF_{12}(t)$ and in the impulse response function $IRF_{12}(t)$ between the signals of two detectors at the transit time of the propagating perturbations. These functions are estimated as the inverse Fourier transforms of the measured $CPSD_{12}(\omega)$ and $TR_{12}(\omega)$ transfer function, respectively. This way of estimation allows us to filter out unwanted frequency components in the frequency domain.

Now these functions are investigated. Cross spectrum was already presented as the numerator of the transfer function of (8):

$$CPSD_{12}(\omega) = \overline{H_{12}(\omega)}|H_1(\omega)|^2 APSD_\varphi(\omega) + |H_{BG}(\omega)|^2 APSD_{BG}(\omega)$$

Let us denote the two components of the cross spectrum similarly to (10):

$$a(\omega) = |H_1(\omega)|^2 APSD_\varphi(\omega)$$

$$b(\omega) = |H_{BG}(\omega)|^2 APSD_{BG}(\omega). \tag{20}$$

With this notation the cross correlation can be written as:

$$\begin{aligned} CCF_{12}(t) &= \frac{1}{2\pi} \int_\omega CPSD_{12}(\omega) e^{i\omega t} d\omega \\ &= \frac{1}{2\pi} \int_\omega \left(\overline{H_{12}(\omega)}a(\omega) + b(\omega) \right) e^{i\omega t} d\omega \end{aligned} \tag{21}$$

while the impulse response function is calculated as the inverse Fourier transform of (9):

$$\begin{aligned} IRF_{12}(t) &= \frac{1}{2\pi} \int_\omega TR_{12}(\omega) e^{i\omega t} d\omega \\ &= \frac{1}{2\pi} \int_\omega \left(\overline{H_{12}(\omega)}A(\omega) + B(\omega) \right) e^{i\omega t} d\omega \end{aligned} \tag{22}$$

where based on (1):

$$\overline{H_{12}(\omega)} = e^{i\omega\tau_{12}} \tag{23}$$

It can be seen after substituting (23) in (21) and (22), and then using Euler's formula of complex numbers that all the terms resulting in imaginary parts are integrates of odd functions (resulting in zero integral), therefore the results consists of purely real terms:

$$\begin{aligned} CCF_{12}(t) &= \frac{1}{2\pi} \int_\omega a(\omega) \cos(\omega\tau_{12}) \cos(\omega t) d\omega + \frac{1}{2\pi} \\ &\times \int_\omega a(\omega)\sin(\omega\tau_{12})\sin(\omega t) d\omega + \frac{1}{2\pi} \\ &\times \int_\omega b(\omega) \cos(\omega t) d\omega \end{aligned} \tag{24}$$

The impulse response function is formally quite similar:

$$\begin{aligned} IRF_{12}(t) &= \frac{1}{2\pi} \int_\omega A(\omega) \cos(\omega\tau_{12}) \cos(\omega t) d\omega + \frac{1}{2\pi} \\ &\times \int_\omega A(\omega)\sin(\omega\tau_{12})\sin(\omega t) d\omega + \frac{1}{2\pi} \\ &\times \int_\omega B(\omega) \cos(\omega t) d\omega \end{aligned} \tag{25}$$

Some measured cross correlation and impulse response functions are shown in Fig. 11 left and right side, respectively, at different levels of background noise. In order to fulfil this condition, three other detector chains were selected. Therefore, the legends of these graphs show the absolute coordinates of the chains, the first and second two digits corresponding to the y and the x-coordinate, respectively, (for coordinate labels see Fig. 1 centre), the coordinates are followed by the 'N1' or 'N7' detector names separated with slash like in the previous graphs.

Generally, both functions have two local extreme values, one at the τ_{12} transit time of the propagating perturbation produced by the first two terms of the cross correlation function of (24) containing component $a(\omega)$, and the other at 0 s (due to the global background noise) produced by the third term of (24) containing $b(\omega)$. The same applies to the impulse response function of (25) with $A(\omega)$ and $B(\omega)$.

The difference between the formally similar functions of $CCF_{12}(t)$ and $IRF_{12}(t)$ is caused by the division with the auto spectrum in the formula of the impulse response function. Fig. 11 shows how much better the two peaks are emphasized by the impulse response function. The inverse Fourier transform of a steeply decreasing spectrum results in wide and low peaks while a weakly decreasing spectrum yields high and narrow peaks. It becomes more understandable after substituting (23) in the integrals of (21) and (22). After partial integration each terms results in an expression of similar shape as:

$$\begin{aligned} C(t) &= \frac{1}{2\pi} \int\limits_{-\widehat{\omega}}^{\widehat{\omega}} X(\omega) e^{i\omega(t+\tau)} d\omega \\ &= \frac{1}{2\pi} \left[X(\omega) - \frac{i}{t+\tau} e^{i\omega(t+\tau)} \right]_{-\widehat{\omega}}^{\widehat{\omega}} - \frac{1}{2\pi} \frac{i}{t+\tau} \\ &\times \int\limits_{-\widehat{\omega}}^{\widehat{\omega}} X'^{(\omega)} e^{i\omega(t+\tau)} d\omega, \end{aligned} \tag{26}$$
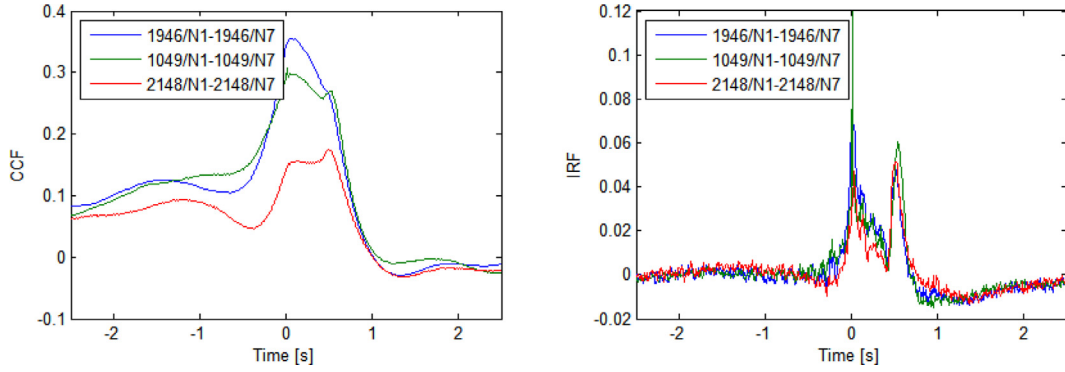
Fig. 11. Cross correlation (left) and impulse response functions (right) at different background noise to perturbation ratios (between the N1 and N7 detectors for three different radial locations).

where $X(\omega)$ denotes $A(\omega)$ and $B(\omega)$ for $CCF_{12}(t)$, and $a(\omega)$ and $b(\omega)$ for $IRF_{12}(t)$, while τ stands τ_{12} with $A(\omega)$ and $a(\omega)$, and τ is 0 with $B(\omega)$ and $b(\omega)$. The first term of (26) always has similar form, the essential difference is caused by the form of $X'(\omega)$. While $a'(\omega) \frac{1}{k^2+\omega^2}$ and $b'(\omega) \frac{1}{k^2+\omega^2}$ for the impulse response function (see Fig. 9), the transfer function terms in the impulse response function are nearly linear, i.e. $A'(\omega)$ and $B'(\omega)$ are constant with a good approximation (as it is shown in Fig. 10). And the integral of the second term of (26) results in Dirac delta for constant $X'(\omega)$.

Let us now look at the forms (24) and (25) of the Fourier transforms. Note that the first and the third term comes from the real part of the integrand, while the second term comes from its imaginary part. The latter does not contain global background noise, and this feature can give the idea to set the real part of the cross spectrum and the transfer function to zero before performing the inverse Fourier transformation. Then only the second terms of (24) and (25) containing no background noise will determine the inverse Fourier transforms. Thus, getting rid of the background noise, we obtain functions centrally symmetrical to the origin that have better readable extreme points at the transit time of the propagating perturbation (see Fig. 12). The values of the transit times (0, 0.51 s, 0.54 s and 0.52 s, in the order of the legend) are in good agreement with the values of Fig. 11, but these peaks are more easily recognizable if programmed methods are to be used.

5. The effect of the measurement arrangement

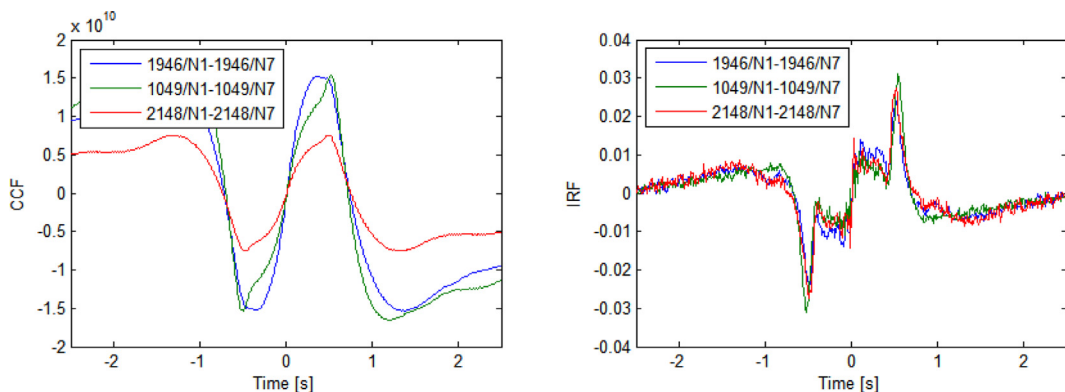In this section the effect of the finite axial size of the detector on the measurement is investigated.

The transfer function of a detector depends on its length and the dependence can be formulated as:

$$H_{\text{det}}(\omega, v, L) = \frac{I(\omega, v, L)}{S(z = z_0, \omega, v)} \tag{27}$$

where L denotes the length of the detector having small cross section compared with its length, v stands for the velocity of the perturbations travelling along the detector, while I is the current produced in the detector by an S noise source reaching the detector.

The space-dependent behaviour of the neutron noise, induced by perturbations generated by the fluctuations of the absorption cross sections and propagating with the coolant of a PWR, were investigated in (Pázsit & Dykin, 2010) in a one-dimensional one-group approximation. They have shown that "in large systems and/or at high frequencies, where the contribution from the reactivity term is negligible, the total noise tends to follow the amplitude and phase of the perturbation". At the end of Section 3 of our paper it was shown that for the VVER-440 reactor this neglect can be done above 1.5 Hz. Accordingly, for the sake of simplicity we assume that the induced noise is proportional to the noise source in the following model calculation.

A $S(z, \omega)$ noise source corresponding to the axially propagating perturbation, at an arbitrary z point of the core in one-dimensional case can be expressed as (Pázsit & Dykin, 2010):

$$S(z, \omega, v) = \frac{\varphi_0(z)}{D} \delta\Sigma_a(0, \omega) e^{-i\omega\frac{z}{v}} \tag{28}$$

where $\varphi_0(z)$ stands for the static neutron flux and $\delta\Sigma_a(0, \omega)$ provides the change of the absorption cross section at the entry point of the core (e.g. due to a temperature fluctuation entering the core)

Fig. 12. Parts of the cross correlation (left) and impulse response functions (right) coming from imaginary parts at different levels of background noise (between the N1 and N7 detectors for three different radial locations).

and v is the coolant velocity. For simplicity it is assumed that the fluctuation is not altered as going through the fuel assembly. Additionally, feedback effects are also neglected. Since the absorption cross section is constant for white noise:

$$S(z, \omega, v) \approx s_0 \varphi_0(z) e^{-i\omega \frac{z}{v}}. \tag{29}$$

The current produced in an infinitesimal small range of a z point of an ideal detector is:

$$\Delta I(z, \omega, v) = S(z, \omega, v) \rho \Delta z = S_0 \varphi_0(z) e^{\frac{-i\omega z}{v}} \rho \Delta z, \tag{30}$$

where S_0 contains s_0 and the proportionality factor between the noise source and the induced noise, while ρ stands for the specific sensitivity of the detector. The v coolant velocity increases with increasing temperature in the core, but here it is approximated by the mean value. Hence, the whole current produced between the starting z_0 and the ending z_1 points of the detector is:

$$I(\omega, v, L) = S_0 \rho \int_{z_0}^{z_1} \varphi_0(z) e^{-i\omega \frac{z}{v}} dz$$

After partial integration:

$$I(\omega, v, L) = S_0 \rho \int_{z_0}^{z_1} \varphi_0(z) \frac{d}{dz} \left(\frac{iv}{\omega} e^{-i\omega \frac{z}{v}} \right) dz$$

$$I(\omega, v, L) = S_0$$
$$\times \frac{iv}{\omega} \rho \left[\varphi_0(z_1) e^{-i\omega \frac{z_1}{v}} - \varphi_0(z_0) e^{-i\omega \frac{z_0}{v}} - \int_{z_0}^{z_1} \varphi_0'(z) e^{-i\omega \frac{z}{v}} dz \right] \tag{31}$$

Finally, in order to express the transfer function of the detector, the current (31) and the white noise source (29) at the entry point of the detector ($z = z_0$) were substituted in (27).

$$H_{\det}(\omega, v, L) = \frac{S_0 \frac{iv}{\omega} \rho \left[\varphi_0(z_1) e^{-i\omega \frac{z_1}{v}} - \varphi_0(z_0) e^{-i\omega \frac{z_0}{v}} - \int_{z_0}^{z_1} \varphi_0'(z) e^{-i\omega \frac{z}{v}} dz \right]}{S_0 \varphi_0(0) e^{-i\omega \frac{z_0}{v}}} \tag{32}$$

$$H_{\det}(\omega, v, L) = \frac{iv\rho}{\omega} \left[\frac{\varphi_0(z_1)}{\varphi_0(z_0)} e^{-i\omega \frac{L}{v}} - 1 - \int_{z_0}^{z_1} \frac{\varphi_0'(z)}{\varphi_0(z_0)} e^{-i\omega \frac{z-z_0}{v}} dz \right] \tag{33}$$

In an environment with constant neutron flux, i.e. where $\varphi_0(z) = \Phi$ and $\varphi_0'(z) = 0$:

$$H_{\det}(\omega, v, L) = \frac{iv\rho}{\omega} \left(e^{-i\frac{\omega L}{2v}} - e^{i\frac{\omega L}{2v}} \right) e^{-i\frac{\omega L}{2v}}$$

$$H_{\det}(\omega, v, L) = \rho L \frac{\sin \frac{\omega L}{2v}}{\frac{\omega L}{2v}} e^{i\frac{\omega L}{2v}} \tag{34}$$

In the above form of the transfer function of the detector for propagating perturbation, the last (exponential) factor stands for frequency dependence of the phase, while the fraction of $\frac{\sin x}{x}$ is responsible for the frequency dependence of the magnitude. This magnitude has zeros depending on the ratio of the detector size and the velocity of the perturbation, where the detector is not sensitive to the perturbation.

In the following section we will show how this transfer function determines the frequency response of an uncompensated neutron detector.

6. Signal components of uncompensated neutron detectors

In this section we will investigate how the two components of the uncompensated Rh SPND signals – the signals produced in the detector and in the cable – relate to each other. We use data of a typical detector chain (06–41) from the end of a fuel cycle. For simplicity, the neutron flux is assumed to be constant (Φ) along the detector chain. The current produced in the detectors is converted to voltage signal with a conversion factor f [V/A]. Thus – in the frequency domain – the voltage generated by the detector is:

$$U_{\det}(\omega) = \Phi f H_{\det}(\omega),$$

After substituting (34).

$$U_{\det}(\omega) = \Phi f H_{\det}(\omega) = U_{\det}^{(\mathrm{DC})} \frac{\sin \frac{\omega L}{2v}}{\frac{\omega L}{2v}} e^{i\frac{\omega L}{2v}}, \tag{35}$$

where $U_{\det}^{(\mathrm{DC})} = \Phi f \rho L$ denotes the non-fluctuating part of the detector signal.

Signals generated in the detector cable (i.e. in the background detector) can be written in a similar way. Since the cable produces only prompt signal, only the prompt component of the detector signal is considered in the comparison.

Based on (35) the frequency response of a (pure) SPND detector and a background detector is shown in Fig. 13 with the sensitivities of the detectors taken into account. The sensitivities vary from detector to detector as it was investigated in (Kiss, Lipcsei, & Házi, Effect of uncompensated SPN detector cables on neutron noise signals measured in VVER-440 reactors, 2003), the figure shows a typical example. The third frequency response (corresponding to the uncompensated SPND) is obtained as the signed sum of the signals of the cable and the detector. Note that the cable current and the detector current have opposite signs. It can be seen in Fig. 13 that above 1 Hz the signal resulting from the passing by perturbation in the detector cable of 2 m length is less than 20% of the signal generated in the detector itself. The transfer function of the detectors is 0 at the values of $\frac{\omega L}{2v} = n\pi, n = 1, 2, \ldots$, i.e. at integer multiples of 1.75 Hz for the cable, and of 17.5 Hz for the detectors.

Fig. 13 shows that the effect of the cable current can only be neglected above 1.0–1.5 Hz in the measurement of propagating perturbations (the exact threshold depends on the ratio of the sensitivities of the detector and the cable). However, the global neutron flux fluctuation (background noise) is proportional to the neutron flux at any point of the cable and the detector, therefore the effect of the cable current cannot be neglected in the detector signal considering the global noise. In the vicinity of singular points (i.e. the zero points of (35)) the fluctuating signal part is suppressed by the noise of the measuring equipment and the background noise, therefore the effect of the propagating perturbation is not measurable here, as the useful signal disappears in the background noise.

7. Effect of the neutron flux distribution on the transfer function of the finite long detector

The shape of the axial neutron flux in the reactor core significantly changes with burnup: the axial flux distribution being nearly cosine at the reactor start-up becomes more and more flat as fuel burnup progresses. Fig. 14 shows characteristic axial neutron flux distributions at the beginning, the middle and the end of a fuel cycle:

Since the detector signal generated by propagating perturbations travelling along the detector depends on the neutron flux, therefore we investigated the effect of the neutron flux shape on the transfer function of the detector with finite length. Since the 20 cm length of the SPNDs is short enough compared to the 242 cm height of the reactor core, the shape of the flux is approximately linear along the detector.
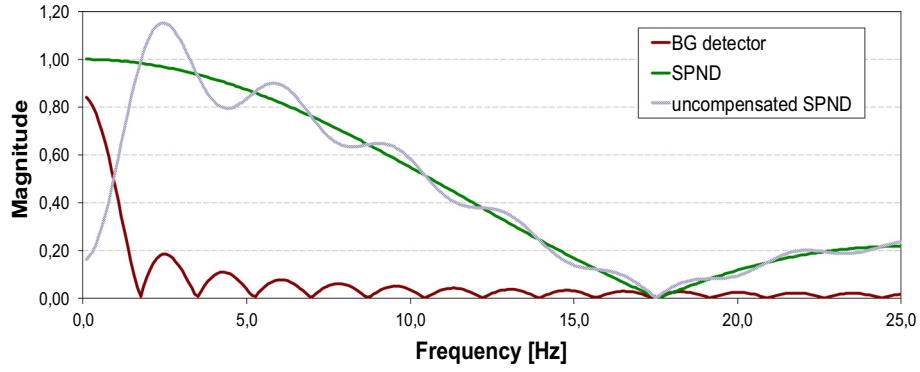
Fig. 13. Frequency response of a 202 cm long background detector (cable), a 20 cm long SPND and an uncompensated SPND for perturbations passing along the detectors.
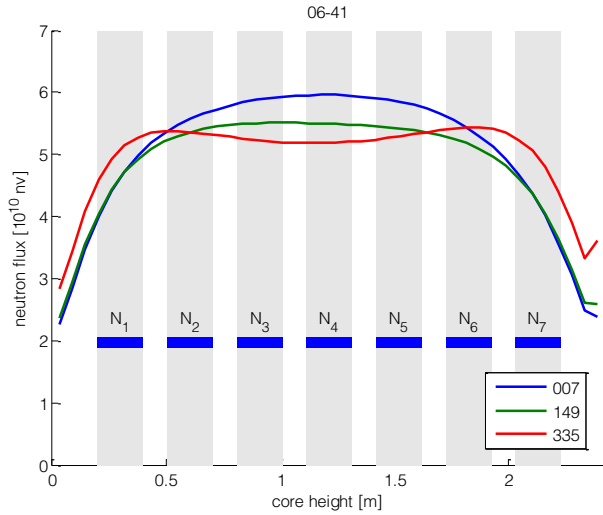

Fig. 14. Axial distribution of the neutron flux during the fuel cycle (legend: effective full power days).

Let $\varphi_0'(z) = m$ and $\varphi_0(z) > 0$, then starting with (33), after substitution, taking the integral, rearranging the equation and using that $m = \frac{\varphi_0(z_1) - \varphi_0(z_0)}{L}$, we get:

$$H_{\det}(\omega, v, L) = \frac{iv\rho}{\omega} \left\{ \frac{\varphi_0(z_1)}{\varphi_0(z_0)} e^{-i\omega\frac{L}{v}} - 1 - \frac{iv}{\omega L}\left(\frac{\varphi_0(z_1)}{\varphi_0(z_0)} - 1\right)\left(e^{-i\omega\frac{L}{v}} - 1\right)\right\} \quad (36)$$

Alternatively, with the separation of real and imaginary parts using Euler's formula of complex numbers, it can be written as:

$$H_{\det}(\omega, v, L) = \frac{v\rho}{\omega}\left\{\frac{\varphi_0(z_1)}{\varphi_0(z_0)}\sin\frac{\omega L}{v} - \frac{2v}{\omega L}\left(\frac{\varphi_0(z_1)}{\varphi_0(z_0)} - 1\right)\sin^2\frac{\omega L}{2v}\right\} + i$$
$$\times \frac{v\rho}{\omega}\left\{\frac{\varphi_0(z_1)}{\varphi_0(z_0)}\cos\frac{\omega L}{v} - 1 - \frac{v}{\omega L}\left(\frac{\varphi_0(z_1)}{\varphi_0(z_0)} - 1\right)\sin\frac{\omega L}{v}\right\}$$

The magnitude and phase of the transfer function is shown in Fig. 15 as the neutron flux changes axially, i.e. for different values of the ratio $\varphi_0(z_1)/\varphi_0(z_0)$. The magnitude changes according to the
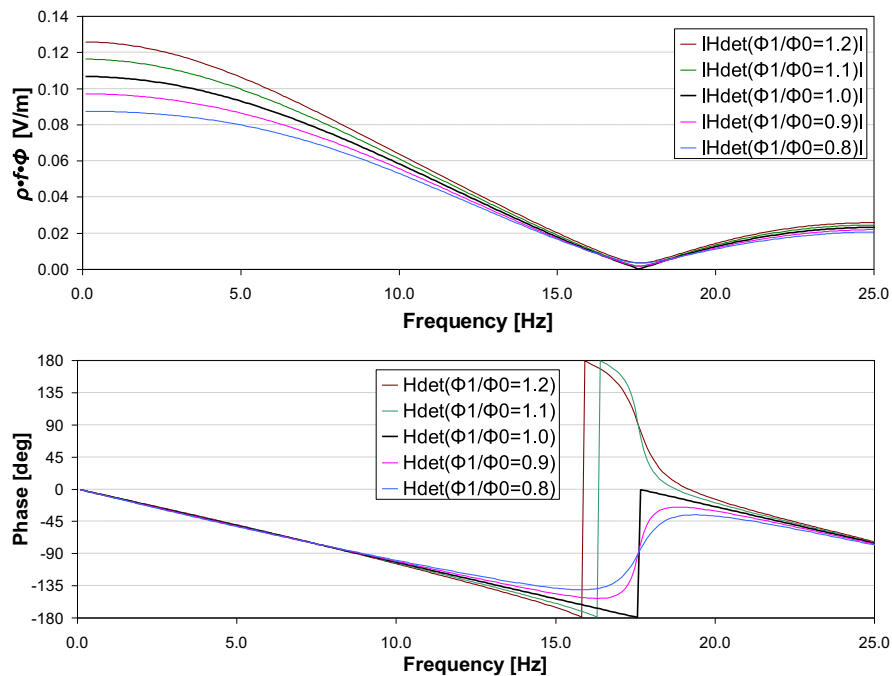

Fig. 15. Absolute value (top) and phase (bottom) of the transfer function of the detector at different values of the ratio $\varphi_0(z_1)/\varphi_0(z_0)$ (denoted as Φ1/Φ0 in the legend).

average neutron flux along the detector, the zero points of the functions are still at integer multiples of 17.5 Hz not depending on the shape of the flux.

Fig. 15 shows that $\varphi_0(z_1)/\varphi_0(z_0)$ does not influence the sink of the magnitude, however the magnitude is zero at the sink only for constant flux (where $\varphi_0(z_1)/\varphi_0(z_0) = 1$), and similarly the phase function has discontinuity only for constant flux.

8. The effect of the neutron flux distribution on the measurement of the transit time

In this section we examine the effect of the non-constant axial neutron flux distribution on the correlation function-based determination of the transit time.

We start from (36) and rearrange it:

$$H_{\text{det}}(\omega, v, L)$$
$$= \frac{iv\rho}{\omega}\left\{\frac{\varphi_0(z_1)}{\varphi_0(z_0)}e^{-i\frac{\omega L}{2v}} - e^{i\frac{\omega L}{2v}} - \frac{iv}{\omega L}\left(\frac{\varphi_0(z_1)}{\varphi_0(z_0)}-1\right)\left(e^{-i\frac{\omega L}{2v}}-e^{i\frac{\omega L}{2v}}\right)\right\}e^{-i\frac{\omega L}{2v}}$$

In the following treatment the two detectors are denoted by indices 1 and 2, so for example z_{20} denotes the front of detector 2 in the direction of flow, while z_{21} stands for its end position. Using the following notation:

$$Q_1 = \frac{\varphi_0(z_{11})}{\varphi_0(z_{10})} \text{ and } Q_2 = \frac{\varphi_0(z_{21})}{\varphi_0(z_{20})}$$

The transfer functions of the two detectors can be written as:

$$H_1 = \frac{iv\rho}{\omega}\left\{Q_1 e^{-i\frac{\omega L}{2v}} - e^{+i\frac{\omega L}{2v}} - \frac{iv}{L\omega}(Q_1-1)\left(e^{-i\frac{\omega L}{2v}}-e^{+i\frac{\omega L}{2v}}\right)\right\}e^{-i\frac{\omega L}{2v}}$$

$$\bar{H}_2 = -\frac{iv\rho}{\omega}\left\{Q_2 e^{+i\frac{\omega L}{2v}} - e^{-i\frac{\omega L}{2v}} + \frac{iv}{L\omega}(Q_2-1)\left(e^{+i\frac{\omega L}{2v}}-e^{-i\frac{\omega L}{2v}}\right)\right\}e^{+i\frac{\omega L}{2v}}$$

and the cross spectrum between the detectors is:

$$NCPSD_{12}(\omega)e^{-i\omega\tau_{12}} = \frac{1}{\rho^2 L^2}H_1\bar{H}_2$$

Let's use the following notations:

$$\text{sinc}x = \begin{cases} \frac{\sin x}{x}, & \text{if } x \neq 0 \\ 1, & \text{if } x = 0 \end{cases}$$

and.

$$\text{cossc}x = \begin{cases} \frac{\cos x - \text{sinc}x}{x}, & \text{if } x \neq 0 \\ 0, & \text{if } x = 0 \end{cases}$$

After substitutions:

$$NCPSD_{12}(\omega) = \frac{1}{\rho^2 L^2}\frac{1}{4}\left\{(Q_1-1)(Q_2-1)\left(\text{cossc}\frac{\omega L}{2v}\right)^2\right.$$
$$+ (Q_1+1)(Q_2+1)\left(\text{sinc}\frac{\omega L}{2v}\right)^2$$
$$\left.-i2(Q_1-Q_2)\text{cossc}\frac{\omega L}{2v}\text{sinc}\frac{\omega L}{2v}\right\}e^{i\omega\tau_{12}}$$

This form can be used to express the cross correlation function:

$$NCCF_{12}(t) = \lim_{\widehat{\omega}\to\infty}\frac{1}{2\pi}\int_{-\widehat{\omega}}^{\widehat{\omega}}\overline{NCPSD_{12}}e^{i\omega t}d\omega$$

The real part of the argument of the limit of the above expression is:

$$\text{Re}\left(\frac{1}{2\pi}\int_{-\widehat{\omega}}^{\widehat{\omega}}\overline{NCPSD_{12}}e^{i\omega t}d\omega\right)$$
$$= \frac{1}{8\pi}\int_{-\widehat{\omega}}^{\widehat{\omega}}(Q_1-1)(Q_2-1)\left(\text{cossc}\frac{\omega L}{2v}\right)^2\cos\omega(t-\tau_{12})$$
$$+ (Q_1+1)(Q_2+1)\left(\text{sinc}\frac{\omega L}{2v}\right)^2\cos\omega(t-\tau_{12})$$
$$- 2(Q_1-Q_2)\text{cossc}\frac{\omega L}{2v}\text{sinc}\frac{\omega L}{2v}\sin\omega(t-\tau_{12})d\omega$$

Graphs of Fig. 16 were obtained by numerical integration of the above expression ($\widehat{f} = \frac{\widehat{\omega}}{2\pi} = 101$Hz; the double of the 50 Hz frequency range of the measurements was applied, in order to have smoother curves, plus 1 Hz was added to avoid possible numerical instabilities). It can be seen that the peaks become asymmetric when the slope of the neutron flux increases. In addition, the position of the slope slightly shifts from the nominal value, but this shift is less than the resolution of the regularly used sampling time (Δt) of our measurements (0.01 s). However, reading the maximum of an asymmetric peak (see e.g. the last graph of Fig. 16) may cause a much bigger systematic error in a noisy environment due to the disturbing signal components making the evaluation more difficult. This error can reach one Δt in our case, which yields a relative error of approximately 2%. The distance between the base points (marked with red '+' signs in Fig. 16) is always $2L/v$.

Peak positions are shown in Fig. 17 for the symmetrical case ($Q_1 = 1/Q_2$), i.e. when the slopes of the axial neutron flux are the same but in opposite direction (three of these peaks are shown in the diagonal from the top left corner to the bottom right corner of Fig. 16). Green markers show the values which can be read at time resolution of 0.001 s.

Fig. 17 shows that the higher the ratio of the neutron flux at the detector ends, the higher the transit time, and although the effect is small, it can influence the measured value due to the resolution of the spectra.

9. Conclusions

This paper investigates analytically the method that has been proven so far for coolant velocity estimation in PWRs and demonstrates its various features through measurements performed at a VVER-440 unit. Presence of the background noise makes the evaluation of the measurements quite difficult, but the disturbing effects can be eliminated.

A model was set up in order to help separating the fractions of the measured signals coming from the propagating perturbation and the background noise, and the spectra of these signal fractions were produced. Then the cross spectrum of the propagating perturbation freed from background noise was reconstructed and the components of the transfer function between the detectors were produced. It was proven that the similarity of the spectra of the background noise and the propagating perturbation makes a sharper peak in the impulse response function than in the cross correlation function.

The transit time is usually read from the cross correlation and impulse response functions estimated as the inverse Fourier transform of the cross spectrum and the transfer function, respectively. We found that resetting the real part (which also contains the background) before performing the inverse Fourier transform produces functions from which the transit time can be read more easily (this helps automation of measurement evaluation).
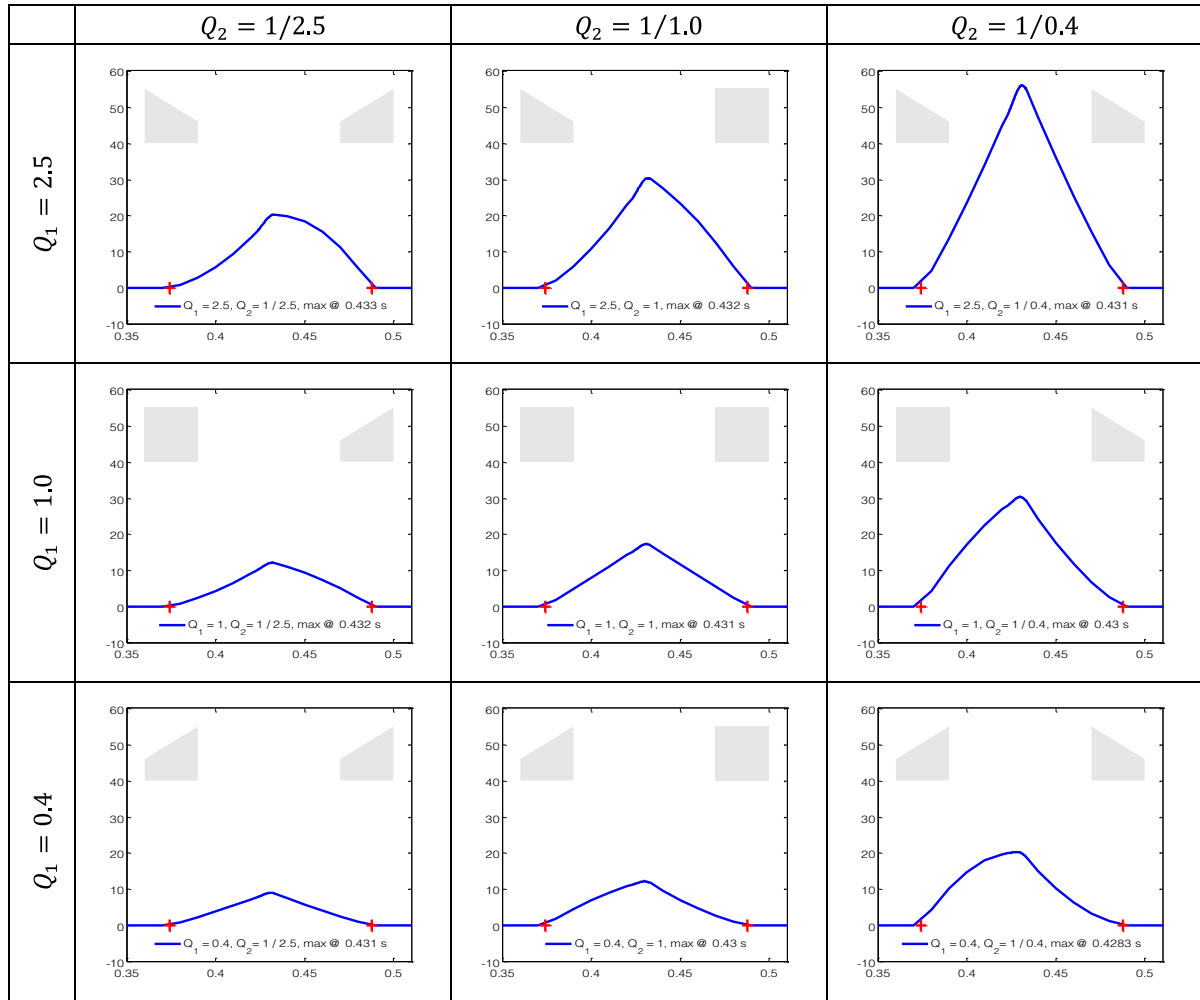
Fig. 16. Calculated shape of the cross correlation function as measurable with detectors in neutron flux with different axial slopes (flux shapes at the detectors are marked with grey icons at the top corners of each graph).
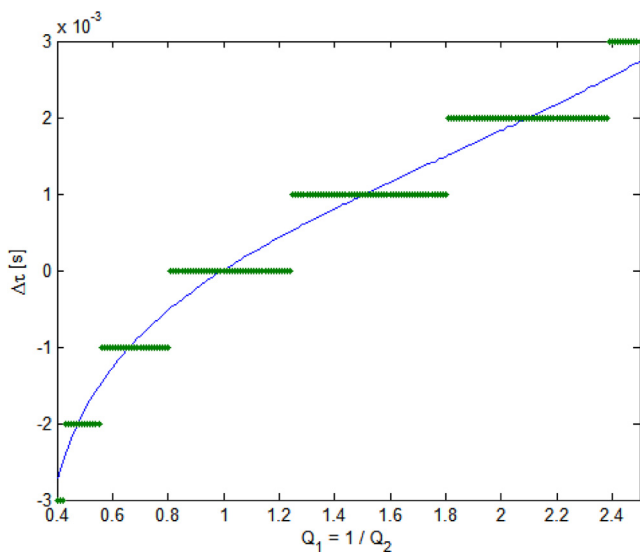

Fig. 17. Time shift of the transit time peaks from the nominal value in the cross correlation function as a function of symmetrical slopes of the neutron flux distribution (green markers: values readable at time resolution of 0.001 s).

It was also investigated how the size of the detector with finite length influences the transfer of the propagating perturbation by the detector. The effect of the non-constant neutron flux distribution along the measurement chain was also investigated and analysed.

Finally, the peaks appearing in the correlation functions at the transit time were investigated and it was found that the slope of axial distribution of the neutron flux makes them asymmetrical and shifts the maximum of the peak slightly.

Neglecting the contribution from the reactivity term in our model applied to describe the effect of the measurement arrangement provides a good approximation above 1.5 Hz. In a future investigation the validity of the detector's transfer function due to its finite size could be extended below 1.5 Hz by using the Green's function of the reactor. A further research may focus on how the shape of the peaks appearing in the impulse response functions depends on the background noise.

Declaration of Competing Interest

Acknowledgements

References

Adorján, F., Czibók, T., Kiss, S., Krinizs, K., Végh, J., 2000. Core Asymmetry Evaluation using Static Measurements and Neutron Noise Analysis. Annals of Nuclear Energy 27, 649–658. https://doi.org/10.1016/S0306-4549(99)00112-7.

Behringer, G., Kosály, G., Kostić, L., 1977. Theoretical Investigation of the Local and Global Components of the Neutron-Noise Field in a Boiling Water Reactor. Nuclear Science and Engineering 63, 306–318. https://doi.org/10.13182/NSE77-A27042.

Behringer, K., Kosály, G., Pázsit, I., 1979. Linear response of the Neutron Field to a Propagating Perturbation of Moderator Density (Two-Group Theory of Boiling Water Reactor Noise). Nuclear Science and Engineering 72, 304–321. https://doi.org/10.13182/NSE79-A20387.

Elter, J. (2005). *Experiment Summary Report: Experimental Investigation of Thermal Mixing Phenomena in a Six Loop VVER Type Reactor, The European project FLOMIX-R: Description of the experimental and numerical studies of flow distribution in reactor primary circuit.* Forshungszentrum Rossendorf, FYR-431: Final report on WP3, Wissenschaftlich-Technishe Beriche.

Kiss, S., Lipcsei, S., 2014. Effect of the steam generator on temperature fluctuations of the primary circuit coolant in VVER-440 reactors. Annals of Nuclear Energy 72, 166–172. https://doi.org/10.1016/j.anucene.2014.05.020.

Kiss, S., Lipcsei, S., 2015. Analysis of propagating temperature perturbations in the primary circuit of PWRs. Annals of Nuclear Energy 85, 1167–1174. https://doi.org/10.1016/j.anucene.2015.08.001.

Kiss, S., Lipcsei, S., 2017. Investigation of circulating temperature fluctuations of the primary coolant in order to develop an enhanced MTC estimator for VVER-440 reactors. Kerntechnik 82, 406–419. https://doi.org/10.3139/124.110813.

Kiss, S., Lipcsei, S., Házi, G., 2003. Effect of uncompensated SPN detector cables on neutron noise signals measured in VVER-440 reactors. Nuclear Engineering and Design 222, 179–192. https://doi.org/10.1016/S0029-5493(02)00323-0.

Kosály, G. (1975). *Investigation of the local component of power-reactor noise via diffusion theory.* Budapest: Central Research Institute for Physics, KFKI-75-27.

Kosály, G., 1980. Noise Investigations in Boiling-Water and Pressurized Reactors. Progr. Nucl. Energy 5, 145–199. https://doi.org/10.1016/0149-1970(80)90004-9.

Lipcsei, S., Kiss, S., & Czibók, T. (2004). A New Generation of Noise Diagnostic Data Acquisition Systems for Paks NPP. Fourth American Nuclear Society International Topical Meeting on Nuclear Plant Instrumentation, Controls and Human-Machine Interface Technologies (NPIC&HMIT), Columbus, Ohio.

Pázsit, I., Demazière, C., 2010. Noise Techniques in Nuclear Systems. In: C. D., . (Ed.), Handbook of Nuclear Engineering. Springer, Boston, MA. https://doi.org/10.1007/978-0-387-98149-9_14.

Pázsit, I., Dykin, V., 2010. Investigation of the space-dependent noise induced by propagating perturbations. Ann. Nucl. Energy 37, 1329–1340. https://doi.org/10.1016/j.anucene.2010.05.014.

Pór, G., Berta, M., Csuvár, M., 2003. Measurement of the Coolant Flow Rate Using Correlation of Temperature Fluctuations. Progress in Nuclear Energy 43, 281–288. https://doi.org/10.1016/S0149-1970(03)00038-6.

Sweeney, F.J., Upadhyaya, B.R., Shieh, D.J., 1985. In-core Coolant Flow Monitoring of Pressurized Water Reactors Using Temperature and Neutron Noise. Progress in Nuclear Energy 15, 201–208. https://doi.org/10.1016/0149-1970(85)90041-1.

Tsimbalov, S.A., 1984. DPZ-1M rhodium neutron detector performance (Russian). Institute of Atomic Energy (IAE), Moscow, USSR.